



Contents lists available at ScienceDirect

# Bioorganic & Medicinal Chemistry Letters

journal homepage: [www.elsevier.com/locate/bmcl](http://www.elsevier.com/locate/bmcl)

## 3D-QSAR and docking studies on pyrazolo[4,3-*h*]quinazoline-3-carboxamides as cyclin-dependent kinase 2 (CDK2) inhibitors

Ping Lan, Wan-Na Chen, Gao-Keng Xiao, Ping-Hua Sun<sup>\*</sup>, Wei-Min Chen<sup>\*</sup>

Guangdong Province Key Laboratory of Pharmacodynamic Constituents of Traditional Chinese Medicine and New Drugs Research, College of Pharmacy, Jinan University, Guangzhou 510632, PR China

### ARTICLE INFO

#### Article history:

Received 25 June 2010

Revised 13 August 2010

Accepted 27 August 2010

Available online 24 September 2010

#### Keywords:

3D-QSAR

CoMFA

CoMSIA

Docking

Cyclin-dependent kinase

### ABSTRACT

3D-QSAR and docking studies were performed on a series of pyrazolo[4,3-*h*]quinazoline-3-carboxamides as CDK2/CyA inhibitors. The CoMFA and CoMSIA models using 54 molecules in the training set, gave  $r^2_{cv}$  values of 0.644 and 0.507,  $r^2$  values of 0.959 and 0.951, respectively. 3D contour maps generated from the two models were applied to identify features important for the activity and better understand the interaction between the inhibitors and the receptor. Molecular docking was employed to explore the binding mode between these compounds and the receptor, as well as help understanding the structure–activity relationship revealed by CoMFA and CoMSIA. The results provide a useful guideline for the rational design of novel CDKs inhibitors.

© 2010 Elsevier Ltd. All rights reserved.

The cyclin-dependent kinases (CDKs) are a family of serine-threonine protein kinases, which play a crucial role in the cell cycle progression.<sup>1–3</sup> CDKs along with their activating partners, the cyclins (Cy), regulate the cell division cycle progression, neuronal function, differentiation, and apoptosis.<sup>4</sup> These CDKs regulate cell growth and survival by several mechanisms including phosphorylation of various proteins whose function is required over the cell cycle.<sup>2,5</sup> In human cancers, genetic and epigenetic aberrations frequently result in overexpression of cyclins or suppression of CDK inhibitory proteins (CDKIs), which provides tumor cells with a selective growth advantage.<sup>6</sup> It was revealed by genetic studies in mice that normal cells were not dependent on interphase CDKs such as CDK2 and CDK4 for their growth, however, certain tumor cells, depending on their origin and their pathogenic spectrum of mutation, may be sensitive to the inhibitions of CDKs.<sup>3</sup> Thus, CDKs especially CDK2 and CDK4 have been regarded as novel therapeutic targets for cancer chemotherapy.<sup>7</sup> CDKs exert their effect via activation of host proteins through phosphorylation of key serine or threonine residues by ATP, therefore, many investigations focused on inhibitors containing key structural hydrogen-bonding motifs to bind to the ATP pocket were carried out.<sup>8–12</sup> A series of pyrazolo [4,3-*h*]quinazoline-3-carboxamides as multi-cyclin-dependent kinase inhibitors were reported by literatures,<sup>2,3</sup> in the present work,

3D-QSAR and docking approaches were applied to study these compounds.

3D-QSAR methods including comparative molecular field analysis (CoMFA) and comparative molecular similarity indices analysis (CoMSIA), were performed to predict the activities of these inhibitors and provided the regions in space where interactive fields may influence the activity. Docking was employed to explore the binding mode between these compounds and the receptor, as well as to reveal the structure–activity relationship revealed by CoMFA and CoMSIA.

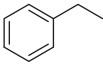
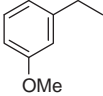
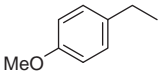
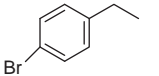
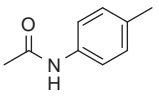
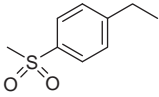
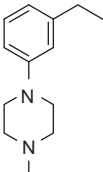
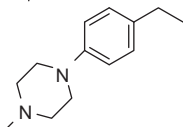
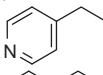
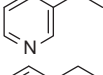
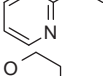
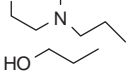
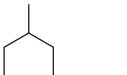
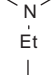

A set of 65 compounds and associated bioactivity data involved in this study were selected from the literature.<sup>2,3</sup> The inhibitory activity data were reported as  $IC_{50}$  against CDK2/CyA. By taking  $\text{Log}(1/IC_{50})$ ,  $IC_{50}$  was converted to  $pIC_{50}$ , and the  $pIC_{50}$  values were used as the dependent variables in all the models subsequently developed. In CoMFA and CoMSIA models, the dataset was randomly segregated into training and test sets comprising 54 and 11 molecules, respectively. (Structures and associated bioactivity values were shown in Tables 1 and 2.)

Structures of entire sets of pyrazolo[4,3-*h*]quinazoline-3-carboxamides were built using SYBYL 8.1 program package of Tripos, Inc.<sup>13</sup> 3D structures of all compounds were constructed using the Sketch Molecule module. Structural energy minimization was performed using the standard Tripos molecular mechanics force field and Gasteiger–Hückel charge, the max iterations for the minimization was set to 2000. The minimization was terminated when the energy gradient convergence criterion of 0.05 kcal/mol Å was reached.<sup>14,15</sup> All of the structures were aligned into a lattice box

<sup>\*</sup> Corresponding authors. Tel.: +86 2085224497; fax: +86 2085224766.

E-mail addresses: [Pinghuasunny@163.com](mailto:Pinghuasunny@163.com) (P.-H. Sun), [twmchen@jnu.edu.cn](mailto:twmchen@jnu.edu.cn) (W.-M. Chen).

**Table 1**  
The Structures of the training and test set molecules

Compd. No.	Substituent				
	R <sup>1</sup>	R <sup>2</sup>	R <sup>3</sup>	R <sup>4</sup>	R <sup>5</sup>
<b>1</b>	NH <sub>2</sub>	CH <sub>3</sub>		—	—
<b>2</b>	NH <sub>2</sub>	CH <sub>3</sub>		—	—
<b>3</b>	NH <sub>2</sub>	CH <sub>3</sub>		—	—
<b>4</b>	NH <sub>2</sub>	CH <sub>3</sub>		—	—
<b>5</b>	NH <sub>2</sub>	CH <sub>3</sub>		—	—
<b>6</b>	NH <sub>2</sub>	CH <sub>3</sub>		—	—
<b>7</b>	NH <sub>2</sub>	CH <sub>3</sub>		—	—
<b>8</b>	NH <sub>2</sub>	CH <sub>3</sub>		—	—
<b>9</b>	NH <sub>2</sub>	CH <sub>3</sub>		—	—
<b>10</b>	NH <sub>2</sub>	CH <sub>3</sub>		—	—
<b>11</b>	NH <sub>2</sub>	CH <sub>3</sub>		—	—
<b>12</b>	NH <sub>2</sub>	CH <sub>3</sub>		—	—
<b>13</b>	NH <sub>2</sub>	CH <sub>3</sub>		—	—
<b>14</b>	NH <sub>2</sub>	CH <sub>3</sub>		—	—
<b>15</b>	NHMe	CH <sub>3</sub>		—	—

(continued on next page)

Table 1 (continued)

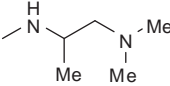
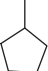
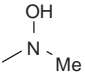
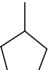
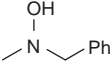
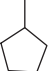
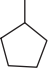
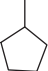
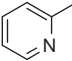
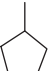
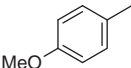
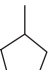
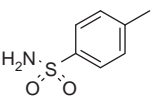
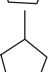
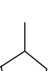
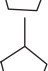
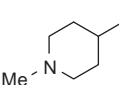

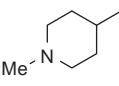
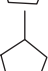
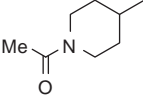
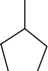
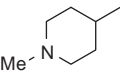
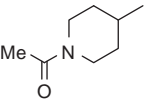
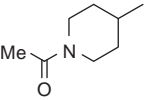
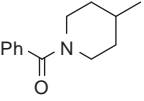
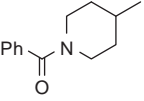
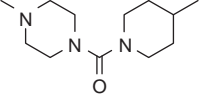
Compd. No.	Substituent				
	R <sup>1</sup>	R <sup>2</sup>	R <sup>3</sup>	R <sup>4</sup>	R <sup>5</sup>
16		CH <sub>3</sub>		—	—
17		CH <sub>3</sub>		—	—
18		CH <sub>3</sub>		—	—
19	NH <sub>2</sub>	PhCH <sub>2</sub>		—	—
20	NH <sub>2</sub>	Ph		—	—
21	NH <sub>2</sub>			—	—
22	NH <sub>2</sub>			—	—
23	NH <sub>2</sub>			—	—
24	NH <sub>2</sub>	HOCH <sub>2</sub> CH <sub>2</sub> CH <sub>3</sub>		—	—
25	NH <sub>2</sub>	F <sub>3</sub> CCH <sub>2</sub> CH <sub>3</sub>		—	—
26	NH <sub>2</sub>			—	—
27	NHMe			—	—
28	NH <sub>2</sub>			—	—
29	NHMe	CH <sub>3</sub>		—	—
30	NH <sub>2</sub>	CH <sub>3</sub>		—	—
31	NHMe	CH <sub>3</sub>		—	—
32	NH <sub>2</sub>	CH <sub>3</sub>		—	—
33	NHMe	CH <sub>3</sub>		—	—
34	NH <sub>2</sub>	CH <sub>3</sub>		—	—

Table 1 (continued)

Compd. No.	Substituent				
	R <sup>1</sup>	R <sup>2</sup>	R <sup>3</sup>	R <sup>4</sup>	R <sup>5</sup>
35	NHMe	CH <sub>3</sub>		—	—
36	NH <sub>2</sub>	CH <sub>3</sub>		—	—
37	NHMe	CH <sub>3</sub>		—	—
38	NH <sub>2</sub>	CH <sub>3</sub>		—	—
39	NHMe	CH <sub>3</sub>		—	—
40	NH <sub>2</sub>	CH <sub>3</sub>		—	—
41	NHMe	CH <sub>3</sub>		—	—
42	NHMe	CH <sub>3</sub>		—	—
43		CH <sub>3</sub>		—	—
44		CH <sub>3</sub>		—	—
45		CH <sub>3</sub>		—	—
46		CH <sub>3</sub>		—	—
47	NH <sub>2</sub>	CH <sub>3</sub>	—		H
48	NH <sub>2</sub>	CH <sub>3</sub>	—	H	
49	NH <sub>2</sub>	CH <sub>3</sub>	—		H
50	NH <sub>2</sub>	CH <sub>3</sub>	—	H	H
51	NH <sub>2</sub>	CH <sub>3</sub>	—		H
52	NHMe	CH <sub>3</sub>	—		H
53	NHMe	CH <sub>3</sub>	—	H	
54	NHMe	CH <sub>3</sub>	—		H
55	NHMe	CH <sub>3</sub>	—	H	

(continued on next page)

**Table 1** (continued)

Compd. No.	Substituent				
	R <sup>1</sup>	R <sup>2</sup>	R <sup>3</sup>	R <sup>4</sup>	R <sup>5</sup>
<b>56</b>	NHMe	CH <sub>3</sub>	—		H
<b>57</b>	NHMe	CH <sub>3</sub>	—	H	
<b>58</b>	NHMe	CH <sub>3</sub>	—		H
<b>59</b>	NHMe	CH <sub>3</sub>	—	H	
<b>60</b>	NHMe	CH <sub>3</sub>	—		H
<b>61</b>	NHMe	CH <sub>3</sub>	—	H	
<b>62</b>	NHMe	CH <sub>3</sub>	—		H
<b>63</b>	NHMe	CH <sub>3</sub>	—	H	
<b>64</b>	NHMe	CH <sub>3</sub>	—		H
<b>65</b>	NHMe	CH <sub>3</sub>	—	H	

**Table 2**

The actual pIC<sub>50</sub>s, predicted pIC<sub>50</sub>s (pred.) and their residuals (res.) of the training and test set molecules

Compd. No.	Actual	CoMFA		CoMSIA	
		Pred.	Res.	Pred.	Res.
<b>1</b>	7.292	7.301	−0.009	7.206	0.086
<b>2</b>	7.181	7.218	−0.037	7.226	−0.045
<b>3<sup>*</sup></b>	7.237	7.233	0.004	7.323	−0.086
<b>4</b>	7.092	7.103	−0.011	7.026	0.066
<b>5</b>	7.886	7.833	0.053	8.020	−0.134
<b>6</b>	7.420	7.473	−0.053	7.677	−0.257
<b>7<sup>*</sup></b>	6.983	7.514	−0.531	7.394	−0.411
<b>8</b>	7.770	7.813	−0.043	7.821	−0.051
<b>9<sup>*</sup></b>	7.678	8.224	−0.546	7.731	−0.053
<b>10<sup>*</sup></b>	7.678	6.884	0.794	7.180	0.498
<b>11</b>	7.061	6.956	0.105	6.977	0.083
<b>12</b>	6.680	6.743	−0.063	6.478	0.202
<b>13</b>	7.721	7.693	0.028	7.483	0.238
<b>14</b>	6.827	6.788	0.039	6.980	−0.153
<b>15</b>	7.013	7.058	−0.045	7.006	0.007
<b>16</b>	5.755	5.642	0.113	5.810	−0.055
<b>17<sup>*</sup></b>	6.757	6.364	0.393	6.649	0.108
<b>18</b>	5.863	5.606	0.257	5.679	0.184
<b>19</b>	7.638	7.661	−0.023	7.652	−0.014
<b>20</b>	7.699	8.053	−0.354	7.967	−0.268
<b>21<sup>*</sup></b>	7.284	7.659	−0.375	7.946	−0.662
<b>22</b>	8.222	8.197	0.025	8.051	0.171
<b>23<sup>*</sup></b>	8.301	8.180	0.121	8.005	0.296
<b>24</b>	8.097	8.019	0.078	8.267	−0.170
<b>25</b>	8.301	8.136	0.165	8.201	0.100
<b>26<sup>*</sup></b>	8.222	8.095	0.127	8.505	−0.283
<b>27</b>	7.229	6.933	0.296	7.101	0.128
<b>28</b>	8.155	8.302	−0.147	8.520	−0.365
<b>29</b>	5.339	5.367	−0.028	5.641	−0.302
<b>30</b>	8.699	8.686	0.013	8.541	0.158
<b>31</b>	7.495	7.355	0.140	7.138	0.357
<b>32</b>	8.523	8.677	−0.154	8.833	−0.310
<b>33</b>	7.602	7.542	0.060	7.430	0.172
<b>34</b>	7.921	7.747	0.174	7.708	0.213
<b>35</b>	5.950	6.122	−0.172	6.313	−0.363
<b>36</b>	9.000	8.980	0.020	8.944	0.056

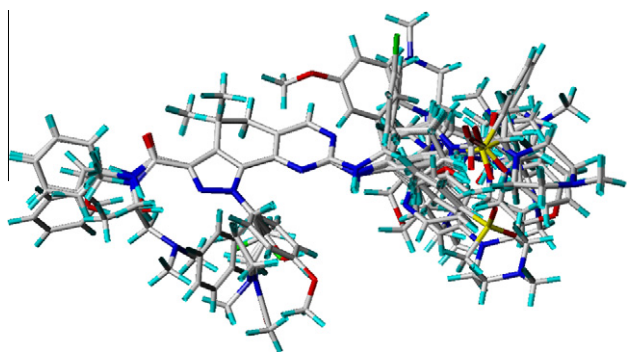
**Table 2** (continued)

Compd. No.	Actual	CoMFA		CoMSIA	
		Pred.	Res.	Pred.	Res.
<b>37</b>	7.237	7.348	−0.111	7.448	−0.211
<b>38</b>	9.000	9.100	−0.100	8.982	0.018
<b>39</b>	8.699	8.714	−0.015	8.429	0.270
<b>40</b>	8.398	8.228	0.170	8.313	0.085
<b>41<sup>*</sup></b>	8.301	7.834	0.467	7.743	0.558
<b>42</b>	7.721	7.594	0.127	7.341	0.380
<b>43</b>	7.092	7.144	−0.053	7.077	0.015
<b>44</b>	7.131	7.076	0.055	7.176	−0.045
<b>45</b>	6.241	6.648	−0.407	6.358	−0.117
<b>46</b>	5.978	6.321	−0.343	5.972	0.006
<b>47</b>	8.699	8.359	0.340	8.593	0.106
<b>48</b>	9.000	8.736	0.264	8.914	0.086
<b>49</b>	7.854	8.335	−0.481	7.959	−0.105
<b>50</b>	7.620	7.512	0.108	7.376	0.244
<b>51</b>	7.770	7.907	−0.137	8.051	−0.281
<b>52</b>	7.347	7.318	0.029	7.404	−0.057
<b>53</b>	7.509	7.210	0.299	7.359	0.150
<b>54</b>	6.863	7.045	−0.182	6.783	0.080
<b>55</b>	6.606	6.432	0.174	6.728	−0.123
<b>56<sup>*</sup></b>	7.538	7.733	−0.195	7.049	0.489
<b>57</b>	7.328	7.293	0.035	7.298	0.030
<b>58</b>	7.260	7.318	−0.058	7.258	0.002
<b>59</b>	7.229	7.251	−0.022	7.261	−0.032
<b>60</b>	7.444	7.396	0.048	7.698	−0.254
<b>61</b>	6.796	6.837	−0.041	6.736	0.060
<b>62</b>	7.229	7.130	0.099	6.969	0.260
<b>63</b>	6.658	6.889	−0.231	6.955	−0.297
<b>64</b>	7.456	7.442	0.014	7.454	0.002
<b>65<sup>*</sup></b>	7.081	6.972	0.109	6.927	0.154

<sup>\*</sup> Test set molecules.

by fitting with pyrazolo[4,3-*h*]quinazoline group as a common structure using compound **38** as a template, which was one of the most active compounds. The aligned molecules were shown in [Figure 1](#).

In the CoMFA method a sp<sup>3</sup> hybridized carbon atom with a charge of 1e served as the probe atom to calculate steric and



**Figure 1.** Alignment of the compounds used in the training set.

electrostatic fields, in which their energy values were truncated at 30 kcal/mol.<sup>16–19</sup> The CoMSIA method incorporating steric, electrostatic, hydrophobic, hydrogen bond donor and acceptor fields was used for the analysis. A  $sp^3$  hybridized carbon atom was used as a probe atom to generate steric field energies and a charge of +1.0 to generate electrostatic field energies. Other similarity indices descriptors were calculated using a  $sp^3$  hybridized carbon atom as a probe atom with a +1 hydrophobicity, +1 H-bond donor, and +1 H-bond acceptor properties.<sup>13</sup> The attenuation factor was set to the default value of 0.3.<sup>20</sup>

Partial Least Squares (PLS) was used to linearly correlate the CoMFA and CoMSIA fields to the  $pIC_{50}$  values. The performance of both the CoMFA and CoMSIA models were evaluated using the leave-one-out (LOO) method.<sup>21</sup> PLS was conjunct with the cross-validation to determine the optimum number of components (ONC) which were then used in deriving the final CoMFA and CoMSIA model without cross-validation. The ONC usually corresponds to the highest cross-validated correlation coefficient ( $r_{cv}^2$ ).<sup>22</sup> After obtaining the optimum number of components, a PLS analysis was then performed with no validation and column filtering 2.0 to generate the highest correlation coefficient ( $r^2$ ).<sup>23</sup> The predictive correlation coefficient ( $r_{pred}^2$ ), based on the molecules of test set, was calculated by the equation shown below:

$$r_{pred}^2 = (SD - PRESS)/SD$$

where, SD is the sum of the squared deviations between the inhibitory activities of the test set and mean activities of the training molecules and PRESS is the sum of squared deviations between predicted and actual activity values for each molecule in the test set.<sup>16,24–26</sup>

**Table 3**  
Results of CoMFA and CoMSIA models

PLS statistics	CoMFA	CoMSIA
$r_{cv}^2$ <sup>a</sup>	0.644	0.507
$r^2$ <sup>b</sup>	0.959	0.951
ONC <sup>c</sup>	6	6
SEE <sup>d</sup>	0.180	0.197
F value <sup>e</sup>	184.167	150.878
$r_{pred}^2$ <sup>f</sup>	0.502	0.462
<b>Field contribution</b>		
Steric	0.516	0.185
Electrostatic	0.484	0.215
Hydrophobic	—	0.279
H-bond donor	—	0.124
H-bond acceptor	—	0.198

<sup>a</sup> Cross-validated correlation coefficient.

<sup>b</sup> Non-cross-validated coefficient.

<sup>c</sup> Optimal number of components.

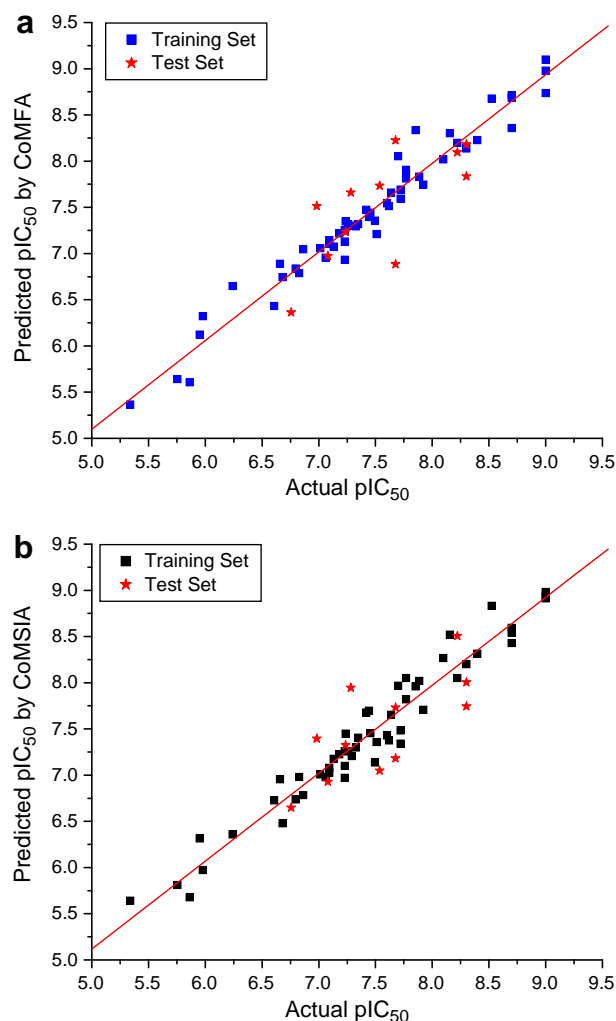
<sup>d</sup> Standard error of estimate.

<sup>e</sup> F-test value.

<sup>f</sup> Predictive correlation coefficient.

The statistical parameters associated in CoMFA and CoMSIA models were listed in Table 3. The CoMFA model gave a cross-validated correlation coefficient ( $r_{cv}^2$ ) of 0.644 (>0.5) with an optimized component of 6. A high non-cross-validated correlation coefficient ( $r^2$ ) of 0.959 with a low standard error estimate (SEE) of 0.180, F value of 184.167 and predictive correlation coefficient ( $r_{pred}^2$ ) of 0.502 were obtained. Contributions of steric and electrostatic fields were 0.516 and 0.484, respectively. The CoMSIA model using steric, electrostatic, hydrophobic, hydrogen bond donor and acceptor fields gave a cross-validated correlation coefficient ( $r_{cv}^2$ ) of 0.507 (>0.5) with an optimized component of 6. A high non-cross-validated correlation coefficient ( $r^2$ ) of 0.951 with a standard error estimate (SEE) of 0.197, F value of 150.878 and predictive correlation coefficient ( $r_{pred}^2$ ) of 0.463 were obtained. Contributions of each field were 0.185, 0.215, 0.279, 0.124, and 0.198, respectively. The actual and predicted  $pIC_{50}$  values and their residual values for the training set and test set compounds were given in Table 2. The relationship between actual and predicted  $pIC_{50}$  of the training set and test set compounds in CoMFA and CoMSIA were illustrated in Figure 2a and b, respectively.

To visualize the information content of the derived 3D-QSAR model, CoMFA contour maps were generated to rationalize the regions in 3D space around the molecules where changes in the steric and electrostatic fields were predicted to increase or decrease the activity. The CoMFA steric and electrostatic contour maps were



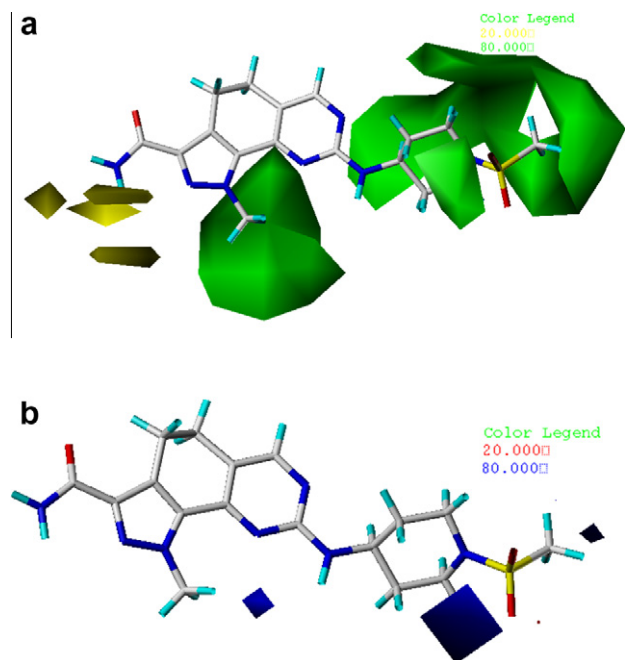
**Figure 2.** Graph of actual versus predicted  $pIC_{50}$  of the training set and the test set using CoMFA (a) and CoMSIA (b).

shown in Figure 3a and b using compound **38** as a reference structure.

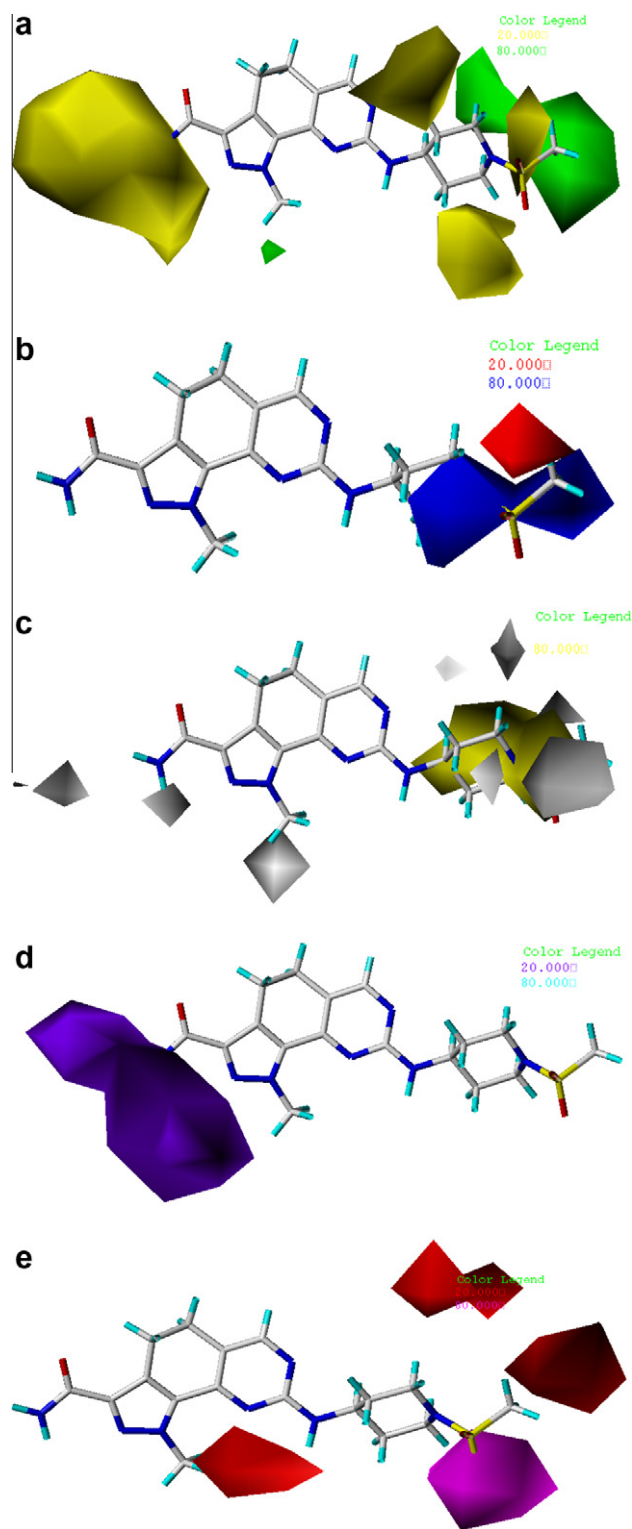
The steric field is represented by green and yellow contours, in which green contours indicate regions where bulky group would be favorable, while the yellow contours represent regions where bulky group would decrease the activity. As shown in Figure 3a, four yellow contours near the R<sup>1</sup> position indicated bulky groups at this position would decrease the potency. This may explain why compounds **16–18** which possessed a bulkier group at R<sup>1</sup> position showed significantly decreased activities than those with a –NH<sub>2</sub> group at R<sup>1</sup>. Compared compounds **27, 30, 32, 34, 36, 38**, and **40** which possessed a –NHMe at R<sup>1</sup> with compounds **31, 33, 35, 37, 39**, and **41** which possessed a –NH<sub>2</sub>, it could be easily found that their activity discrepancies can be explained by these yellow contours. A big green contour near the R<sup>2</sup> position suggested that bulky group at this position would be favored. By checking all N-1 modified molecules, it was found that compounds **22–26** with a bulkier substituent at R<sup>2</sup>, were the most potential derivatives. Another big green contour around R<sup>3</sup> position also indicated that bulky groups would be favorable. Compounds **22–26, 30, 32, 36, 38–41, 47–48** which were the most active compounds in the database, all possessed a bulky group at this position.

The electrostatic field is indicated by blue and red contours, which demonstrate the regions where electron-donating group and electron-withdrawing group would be favorable, respectively. In Figure 3b, three blue contours near R<sup>2</sup> and R<sup>3</sup> positions indicated that electron-donating substituent may increase the activity. The most potential derivatives, such as compounds **26, 28, 30, 32, 36, 38–41, 47–48**, all possessed an electron-donating group (e.g., methyl, 4-methylpiperidin-1-yl, 4-methylpiperazin-1-yl) at R<sup>2</sup> or R<sup>3</sup> positions.

Figure 4a–e depicted the steric, electrostatic, hydrophobic, hydrogen bond donor and hydrogen bond acceptor contours plots for compound **38**. The steric and electrostatic contours were almost similar to those of CoMFA model.



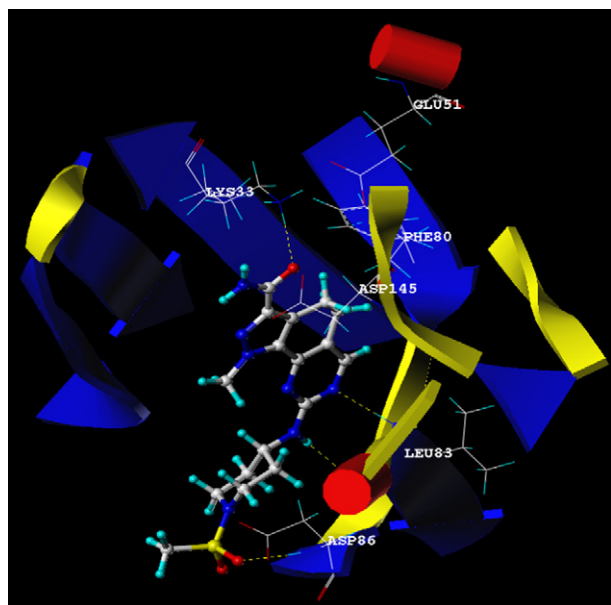
**Figure 3.** Std\* coeff. contour maps of CoMFA analysis with 2 Å grid spacing in combination with compound **38**. (a) Steric fields: green contours (80% contribution) indicate regions where bulky groups increase activity, while yellow contours (20% contribution) indicate regions where bulky groups decrease activity, and (b) electrostatic fields: blue contours (80% contribution) indicate regions where electron-donating groups increase activity, while red contours (20% contribution) indicate regions where electron-withdrawing groups increase activity.



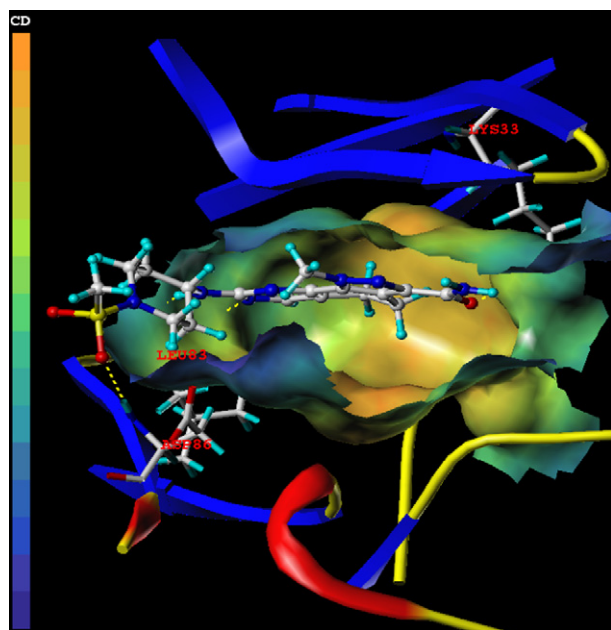
**Figure 4.** Std\* coeff. contour maps of CoMSIA analysis with 2 Å grid spacing in combination with compound **38**. (a) Steric contour map. Green and yellow contours refer to sterically favored and disfavored regions. (b) Electrostatic contour map. Blue and red contours refer to regions where electron-donating and electron-withdrawing groups are favored. (c) Hydrophobic contour map. White contours (20% contribution) refer to regions where hydrophilic substituents are favored; yellow contours (80% contribution) indicate regions where hydrophobic substituents are favored. (d) Hydrogen bond donor contour map. The cyan and purple (80% and 20% contributions) contours indicate favorable and unfavorable hydrogen bond donor groups. (e) Hydrogen bond acceptor contour map. The magenta contours (80%) for hydrogen bond acceptor group increase activity, red contours (20%) indicate the disfavored region.



In hydrophobic field, white and yellow contours highlighted areas where hydrophilic and hydrophobic properties were favored. In Figure 4c, two white contours near R<sup>1</sup> position revealed that hydrophilic group at this region would benefit potency, which stressed the extreme importance of the hydrophilic –NH<sub>2</sub> group. Furthermore, this observation was in agreement with the electrostatic contour map in CoMFA. A big yellow contour along with five white ones around the R<sup>3</sup> position indicated that hydrophobic field at this position was not important for the activity.



**Figure 5.** MOLCAD Robbin surfaces structure of selected compound **38** in complex with the ATP pocket of CDK2/CyA (PDB code: 2WIH). Key residues and hydrogen bonds were labeled. The alpha helices were shown as helices or cylinders, while beta sheets were shown as arrows and the loop regions as tubes.

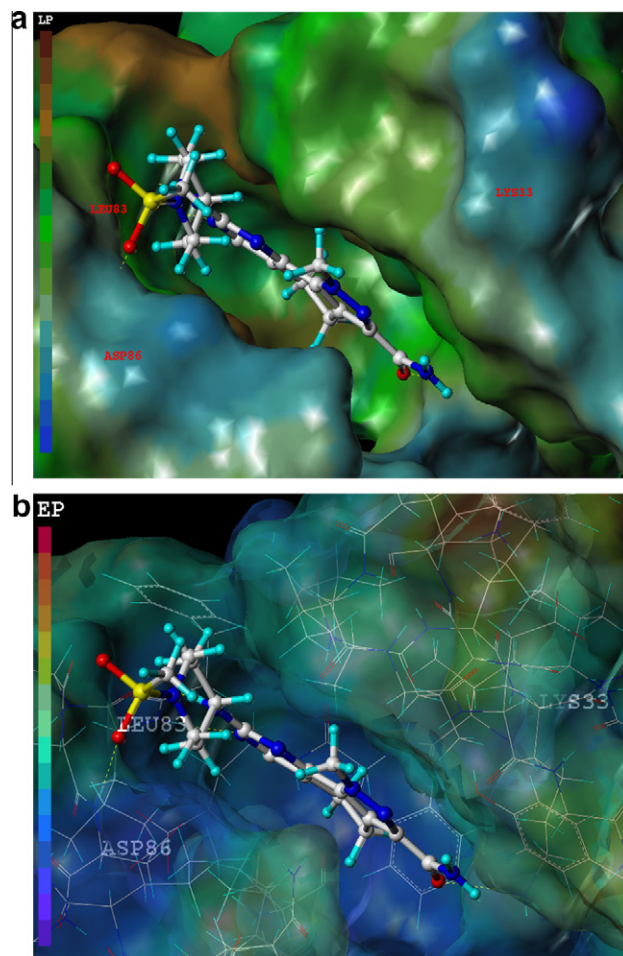


**Figure 6.** The MOLCAD Robbin and Multi-Channel surfaces structure displayed with cavity depth potential of the ATP pocket within the compound **38**. Key residues and hydrogen bonds were labeled. The cavity depth color ramp ranges from blue (low depth values = outside of the pocket) to light red (high depth values = cavities deep inside the pocket).

In hydrogen bond donor field, the cyan and purple contours indicated favorable and unfavorable hydrogen bond donor groups. In Figure 4d, only a big purple contour appeared at the R<sup>1</sup> position which suggested hydrogen bond donor group would be disfavored. In fact, the carbonyl group of C-3 carboxamide acted as hydrogen bond acceptor by forming H-bond with the receptor.

In hydrogen bond acceptor field, the magenta and red contours identified favorable and unfavorable positions for hydrogen bond acceptors, respectively. In Figure 4e, a red contour near N-15 position indicated that a hydrogen bond acceptor substituent would be disfavored, in fact, the –NH groups at this position acted as hydrogen bond donor and formed H-bond with the ATP pocket. A big magenta contour around the methylsulfate group revealed that a hydrogen bond acceptor would increase the potency, the methylsulfate group may act as a hydrogen bond acceptor by forming H-bond with the residues of ATP-binding site of the receptor. Compounds **36**, **38**–**41**, which possessed a hydrogen bond acceptor group at the terminal of R<sup>3</sup> position, showed significantly increased activities.

Crystal structure of CDK2/CyA was retrieved from RCSB Protein Data Bank (PDB entry code: 2WIH). The CDK2/CyA structure was utilized in subsequent docking experiments without energy minimization. The most active compound **38** was docked into corresponding ATP-binding site by an empirical scoring function and a patented search engine in Surflex-Dock.<sup>13</sup> In order to visualize



**Figure 7.** The MOLCAD lipophilic (a) and electrostatic (b) potential surfaces of ATP-binding site of CDK2/CyA (PDB code: 2WIH) within the compound **38**. Key residues and hydrogen bonds were labeled. In (a), the brown represents highest lipophilic area while blue indicated highest hydrophilic area. In (b), the red color shows the electron-withdrawing zone and purple color shows electron-donating zone.



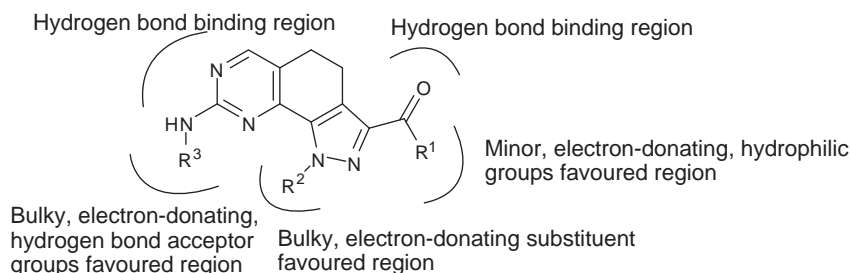


Figure 8. Structure–activity relationship revealed by 3D-QSAR and docking.

secondary structure elements and the cavities and channels of the ATP pocket, the MOLCAD Robbin and Multi-Channel surfaces program were applied. The secondary structure and cavity of the ATP pocket within the selected compound **38** were shown in Figure 5. As shown in Figure 5, the N-9 and N-15 acted as the hydrogen bond acceptor and donor, formed H-bond with the –NH and –OH group of Leu83 residue, respectively. The carbonyl group at C-14 position formed H-bond with –NH<sub>2</sub> group of Lys33 residue. The methylsulfate group acted as a hydrogen bond acceptor by binding to the –NH group of Asp86. The results confirmed the observation from the CoMSIA hydrogen bond donor and acceptor contour maps.

Figure 6 depicted the MOLCAD cavity depth potential surface of the binding site of CDK2/CyA within compound **38**, the cavity depth color ramp ranges from blue (low depth values = outside of the pocket) to light red (high depth values = cavities deep inside the pocket). As shown in Figure 6, the whole molecule except the R<sup>3</sup> position was in the light red area which indicated that the majority parts of compound **38** were anchored to the deep inside the ATP pocket.

The MOLCAD molecule surfaces of the ATP-binding site were also developed and displayed with lipophilic and electrostatic potential to examine the hydrophobic contour map of CoMSIA and the electrostatic contour map of CoMFA. In Figure 7a, the brown represents highest lipophilic area of the molecule while blue indicated highest hydrophilic area, the R<sup>1</sup> position of compound **38** was found in the hydrophilic blue area. In Figure 7b, the red color shows the electron-withdrawing zone and purple color shows electron-donating zone, and compound **38** was anchored into an electron-donating blue area. The observations obtained from Figure 6 satisfactorily matched the corresponding contour maps.

The structure–activity relationship revealed by 3D-QSAR and docking studies was illustrated in Figure 8. In detail, the minor, electron-donating groups at R<sup>1</sup> position are favorable; the bulkier, electron-donating groups at R<sup>2</sup> position may benefit the potency; the bulkier, electron-donating and hydrogen bond acceptor substituent at R<sup>3</sup> position would increase the activity. The N-7 and N-15 atoms were essential for binding to the ATP pocket.

In this study, 3D-QSAR and molecular docking studies were performed on a series of CDK2/CyA inhibitors. In 3D-QSAR studies, both the CoMFA and CoMSIA analyses gained some insights into the key structural factors affecting the bioactivity of these inhibitors. The excellent predictive ability of the developed CoMFA and CoMSIA models indicated that they can be used for predicting the IC<sub>50</sub> values of pyrazolo[4,3-*h*]quinazoline-3-carboxamides prior to synthesis. Furthermore, the CoMFA and CoMSIA contour maps along with the docking results offered enough information to understand the structure–activity relationship and identify structural features influencing the inhibitory activity. The correlation of the results obtained from 3D-QSAR and docking studies can be served as a useful guideline for the further modification of pyrazolo[4,3-*h*]quinazoline-3-carboxamides that function as CDK2/CyA inhibitors.

## Acknowledgments

This research work is supported by the Natural Science Foundation of Guangdong Province (No. 9151063201000053) and the Fundamental Research Funds for the Central Universities (No. 2161 0405), China.

## References and notes

- Wyatt, P. G.; Woodhead, A. J.; Berdini, V.; Boulstridge, J. A.; Carr, M. G.; Cross, D. M.; Davis, D. J.; Devine, L. A.; Early, T. R.; Feltell, R. E.; Lewis, E. J.; McMenamin, R. L.; Navarro, E. F.; O'Brein, M. A.; O'Reilly, M.; Reule, M.; Saxty, G.; Seavers, L. C. A.; Smith, D.-M.; Squires, M. S.; Trewartha, G.; Walker, M. T.; Woolford, J.-A. *A. J. Med. Chem.* **2010**, *51*, 4986.
- Traquandi, G.; Ciomei, M.; Ballinari, D.; Casale, E.; Colombo, N.; Croci, V.; Fiorentini, F.; Isacchi, A.; Longo, A.; Mercurio, C.; Panzeri, A.; Pastori, W.; Pevarello, P.; Volpi, D.; Roussel, P.; Vulpetti, A.; Brasca, M. G. *J. Med. Chem.* **2010**, *53*, 2171.
- Brasca, M. G.; Amboldi, N.; Ballinari, D.; Cameron, A.; Casale, E.; Cervi, G.; Colombo, M.; Colotta, F.; Croci, V.; D'Alessio, R.; Fiorentini, F.; Isacchi, A.; Mercurio, C.; Moretti, W.; Panzeri, A.; Pastori, W.; Pevarello, P.; Quartieri, F.; Roletto, F.; Traquandi, G.; Vianello, P.; Vulpetti, A.; Ciomei, M. *J. Med. Chem.* **2009**, *52*, 5152.
- Choi, S.-J.; Lee, J.-E.; Jeong, S.-Y.; Im, I.; Lee, S.-D.; Lee, E.-J.; Lee, S. K.; Kwon, S.-M.; Ahn, S.-G.; Yoon, J.-H.; Han, S.-Y.; Kim, J.-I.; Kim, Y.-C. *J. Med. Chem.* **2010**, *53*, 3696.
- Tsou, H.-R.; Liu, X.; Birnberg, G.; Kaplan, J.; Otteng, M.; Tran, T.; Kutterer, K.; Tang, Z.; Suayan, R.; Zask, A.; Ravi, M.; Bretz, A.; Grillo, M.; McGinnis, J. P.; Rabindran, S. K.; Ayril-Kaloustian, S.; Mansour, T. S. *J. Med. Chem.* **2009**, *52*, 2289.
- McIntyre, N. A.; McInnes, C.; Griffiths, G.; Barnett, A. L.; Kontopidis, G.; Slawin, A. M. Z.; Jackson, W.; Thomas, M.; Zheleva, D. I.; Wang, S.; Blake, D. G.; Westwood, N. J.; Fischer, P. M. *J. Med. Chem.* **2010**, *53*, 2136.
- Ahn, Y. M.; Vogeti, L.; Liu, C.-J.; Santhapuram, H. K. R.; White, J. M.; Vasandani, V.; Mitscher, L. A.; Lushington, G. H.; Hanson, P. R.; Powell, D. R.; Himes, R. H.; Roby, K. F.; Ye, Q.; Georg, G. I. *Bioorg. Med. Chem.* **2007**, *15*, 702.
- Ibrahim, D. A.; El-Metwally, A. M. *Eur. J. Med. Chem.* **2010**, *45*, 1158.
- Singh, S. K.; Dessalew, N.; Bharatam, P. V. *Eur. J. Med. Chem.* **2006**, *41*, 1310.
- Chu, X.-J.; DePinto, W.; Bartkovitz, D.; So, S.-S.; Vu, B. T.; Packman, K.; Lukacs, C.; Ding, Q.; Jiang, N.; Wang, K.; Goelzer, P.; Yin, X.; Smith, M. A.; Higgins, B. X.; Chen, Y.; Xiang, Q.; Moliterni, J.; Kaplan, G.; Graves, B.; Lovey, A.; Fotouhi, N. *J. Med. Chem.* **2006**, *49*, 6549.
- Echalier, A.; Bettayeb, K.; Ferandin, Y.; Lozach, O.; Clement, M.; Valette, A.; Liger, F.; Marquet, B.; Morris, J. C.; Endicott, J. A.; Joseph, B.; Meijer, L. *J. Med. Chem.* **2008**, *51*, 737.
- Richardson, C. M.; Williamson, D. S.; Parratt, M. J.; Borgognoni, J.; Cansfield, A. D.; Dokurno, P.; Francis, G. L.; Howes, R.; Moore, J. D.; Murray, J. B.; Robertson, A.; Surgenor, A. E.; Torrance, C. J. *Bioorg. Med. Chem. Lett.* **2006**, *16*, 1353.
- SYBYL 8.1, Tripos Inc., St. Louis, USA.
- Verma, S. M.; Razdan, B. K.; Sasmal, D. *Bioorg. Med. Chem. Lett.* **2009**, *19*, 3108.
- Pan, X.; Tan, N.; Zeng, G.; Huang, H.; Yan, H. *Eur. J. Med. Chem.* **2010**, *45*, 667.
- Zhang, N.; Zhong, R. *Eur. J. Med. Chem.* **2010**, *45*, 292.
- Gupta, P.; Roy, N.; Garg, P. *Eur. J. Med. Chem.* **2009**, *44*, 4276.
- Geldenhuys, W. J.; Nakamura, H. *Bioorg. Med. Chem. Lett.* **2010**, *20*, 1918.
- Sethi, K. K.; Verma, S. M.; Prasanthi, N.; Sahoo, S. K.; Parhi, R. N.; Suresh, P. *Bioorg. Med. Chem. Lett.* **2010**, *20*, 3089.
- Qin, J.; Lei, B.; Xi, L.; Liu, H.; Yao, X. *Eur. J. Med. Chem.* **2010**, *45*, 2768.
- Teixeira, C.; Serradji, N.; Maurel, F.; Barbault, F. *Eur. J. Med. Chem.* **2009**, *44*, 3524.
- Sheng, C.; Zhu, J.; Zhang, W.; Zhang, M.; Ji, H.; Song, Y.; Xu, H.; Yao, J.; Miao, Z.; Zhou, Y.; Zhu, J.; Lü, J. *Eur. J. Med. Chem.* **2007**, *42*, 477.
- Du-Cuny, L.; Song, Z.; Moses, S.; Powis, G.; Mash, E. A.; Meuillet, E. J.; Zhang, S. *Bioorg. Med. Chem.* **2009**, *17*, 6983.
- Hu, R.; Barbault, F.; Delamar, M.; Zhang, R. *Bioorg. Med. Chem.* **2009**, *17*, 2400.
- Politi, A.; Durdagi, S.; Moutevelis-Minakakis, P.; Kokotos, G.; Papadopoulos, M. G.; Mavromoustakos, T. *Eur. J. Med. Chem.* **2009**, *44*, 3703.
- Yi, P.; Qiu, M. *Eur. J. Med. Chem.* **2008**, *43*, 604.